PAPER

Check for updates

Green synthesis of mesoporous anatase TiO$_2$ nanoparticles and their photocatalytic activities

Sunderishwary S. Muniandy,[a] Noor Haida Mohd Kaus,[b] Zhong-Tao Jiang, [c] Mohammednoor Altarawneh [c] and Hooi Ling Lee [*a]

Titanium dioxide (TiO$_2$) materials have been the focus of many promising applications due to their low-cost, availability and biocompatible properties. In this study, mesoporous anatase TiO$_2$ nanoparticles were synthesised using a green chemistry approach. This visible-light active photocatalyst was prepared *via* a simple and solvent free precipitation method at low temperatures using titanium tetraisopropoxide (TTIP) as a precursor and soluble starch as the template. The effect of initial solution pH and concentration of TTIP on surface morphology and photocatalytic activities of TiO$_2$ nanoparticles were evaluated. Based on the results obtained, the TiO$_2$ nanocatalyst prepared using 0.01 mol of TTIP under basic conditions revealed the best photocatalytic activity. The as-synthesised nanoparticles were further characterised using X-ray powder diffraction (XRD), scanning electron microscopy (SEM) and nitrogen adsorption analysis (NAA). The XRD spectrum confirmed that the catalyst was composed of anatase tetragonal TiO$_2$ phase. The Brunauer–Emmett–Teller (BET) surface area of 81.59 m^2 g^{-1} proved the presence of mesopores (average pore size = 8.7 nm) which partially contributed to and catalysed the photodegradation process of methylene blue (MB) solution under sunlight. The effects of various parameters such as initial dye concentration, catalyst dosage and recyclability of the catalyst were evaluated to determine the best conditions. Results obtained suggest that TiO$_2$ nanoparticles synthesised through the green chemistry approach under optimum conditions exhibited an effective photodegradation process of MB solution under sunlight.

1 Introduction

Titanium dioxide (TiO$_2$) is one of the most extensively studied materials due to its harmless nature and good chemical and thermal stability.[1] Titanium dioxide possesses high potential because of its availability and low cost. It is a binary metal oxide that exists in three different polymorphs; namely anatase, rutile and brookite. These polymorphs exhibit different bandgap energies with rutile TiO$_2$ (3.0 eV), anatase TiO$_2$ (3.2 eV) and brookite TiO$_2$ ($\sim$3.2 eV). In past decades, TiO$_2$ has received great attention for applications such as self-cleaning, solar cells, gas sensors,[2] anti-fogging, deodorisation and waste water remediation due to its superhydrophilic property.[3] Among these applications, photocatalysis is considered to be the most practical due to its usage of sunlight to decompose organic pollutants.[4,5] The mechanism involved in photocatalysis reaction exerted by semiconductors,[6–8] mainly discussed the formation

of free electrons and holes in the conduction and valance band region as explained in the literature.[2,10,20,21]

Many methods such as sol gel route,[9,10] hydrothermal,[11] polyol synthesis,[12] and precipitation[13] had been reported in the synthesis of TiO$_2$ nanoparticles (NPs). Among these methods, the sol–gel technique employed a low temperature process. However, the end product would contain high carbon content when organic reagents are used during the experiments. Hydrothermal methods have been used to synthesise metal oxides directly from solution but most of the earlier studies done on synthesis of TiO$_2$ NPs using a hydrothermal method required high temperatures which resulted in the formation of polydispersed powders.[12] The polyol process is the most well-known method among the production of metal oxides. Even though this process is able to control various particles property, it employs large amount of polyhydroxy alcohol (solvent) which makes this synthetic route environmentally unfavourable and unsafe. Up to this point in time, very little work has been reported on the synthesis of TiO$_2$ NPs under the precipitation process using the green chemistry approach.

Green chemistry denotes the implementation of chemical processes and products to reduce the use of substances hazardous towards human and the environment.[14] Non-toxic solvents, closed reactors, and harmless waste production are

[a]*Nanomaterials Research Group, School of Chemical Sciences, Universiti Sains Malaysia, Penang, Malaysia. E-mail: hllee@usm.my*
[b]*Nano Hybrid Materials Group, School of Chemical Sciences, Universiti Sains Malaysia, Penang, Malaysia*
[c]*Surface Analysis and Materials Engineering Research Group, School of Engineering & Information Technology, Murdoch University, Murdoch, WA 6150, Australia*

normally the factors used in order to reduce the impact on environment by easing waste disposal. Thus, a method can be recognised as a green technique if any previous method was altered according to the twelve principles of the 'Green Chemistry Principles'.[15] Designing a method, according to green chemistry principles, results in an economical, safer, non-toxic and simpler route of synthesis. Therefore, green synthesis of NPs is considered an improved approach as it is environmentally friendly, sustainable, and relatively reproducible and the end products are often more stable.[16]

In this article, the focus is on developing a green technique adopting the fast precipitation method at a low temperature to synthesise TiO_2 Nanoparticles (NPs) using titanium tetraisopropoxide as the source of titanium, water as solvent and starch as template. It is postulated that this modified method minimises the impact on the safety of living organism and the environment. The effects of the pH and concentration of the precursor on TiO_2 NPs and their potential on self-cleaning application were also explored.

2 Experimental

2.1 Materials

Titanium(IV) tetraisopropoxide, TTIP ≥97% purity (Sigma-Aldrich, Co., USA), soluble starch (System), ammonium hydroxide, NH_4OH (Fluka Analyticals, Sigma-Aldrich, Co., Germany), purchased pure anatase, ≥99% (Sigma-Aldrich, Co., USA), methylene blue, MB (QREC, Grade AR, (Asia) Sdn. Bhd, Malaysia). All reagents were used as purchased and without further purification.

2.2 Synthesis of TiO_2 nanoparticles

The TiO_2 NP was synthesised based on the ZnO synthesis work by Zhang and the co-workers[16] with some modifications. In a typical procedure, soluble starch was dissolved in 150 mL of boiling distilled water. Then, 0.01 mol of titanium tetraisopropoxide (TTIP) was added into the starch solution under stirring for 5 min at 85 °C. Yellow solution with white precipitates were formed after adjusting the pH of solution to basic (pH 9.0)/neutral (pH 7.0)/acidic (pH 5.0) by slowly adding ammonium hydroxide ($NH_4(OH)$) solution with constant stirring for 30 min. The resulting precipitate was centrifuged at 8500 rpm for 10 min, followed by several cycles of washing with distilled water and finally dried in an oven at 50 °C. The dried as-obtained powder was further calcined in air at 500 °C for 2 h to obtain TiO_2 nanoparticles (NPs).

2.3 Characterisations of TiO_2 nanoparticles

The crystallinity and phase purity of the synthesised photocatalyst was analysed by powder X-ray diffraction (XRD) (PW 3040/60 X'PERT PRO, PANalytical) using CuK_α (1.541 Å) radiation in the range $2\theta = 10$–$90°$. The specific surface area and pore size distribution studies were measured by nitrogen adsorption isotherms using a N_2 adsorption analyser (NAA) (Micromeritics ASAP 2020 Surface Adsorption Porosimeter (SAP)). The Brunauer–Emmett–Teller (BET) and Barrett–Joyner–Halenda (BJH)

models were used to estimate the surface area and pore size of the TiO_2 NPs. The TiO_2 NPs was further characterised by field emission scanning electron microscope (FESEM) (Leo Supra 50 VP Field Emission SEM) to determine its surface morphology. An acceleration electron voltage of 10 kV voltage was applied to obtain the FESEM images. Further analysis was carried out using high-resolution transmission electron microscopy (HRTEM) (TECNAI G2 20 S-TWIN, FEI) at 200 kV. X-ray photoelectron spectroscopy (XPS) was carried out using high resolution X-ray photoelectron spectroscopy Axis – Ultra DLD, XPS, Kratos with monochromatic AlK_α (1486.6 eV), X-ray radiation (15 kV and 10 mA) and equipped with a hemispherical analyser which operated at 150 W. All the reported binding energy (BE) data were calibrated using the C 1s from C–H at 284.6 eV. Curve fitting was accomplished using CASAXPS (version 2.3.17) and a GL (30) Gaussian (70%)–Lorentzian (30%) profile, and the standard Shirley background was used for fitting the components.

2.4 Evaluation of photocatalytic activities

The photocatalytic activities of the TiO_2 NPs obtained were evaluated *via* the photocatalytic oxidation of methylene blue (MB) under sunlight irradiation. Prior to irradiation, 0.1 g of calcined TiO_2 NPs was dispersed in 200 mL MB (6 mg L^{-1}) and the solution was magnetically stirred for one hour in darkness to reach adsorption equilibrium. The MB solution with photocatalyst was exposed to sunlight (75–120 kLux) for two hours. During irradiation, 10 mL of the mixture was collected and centrifuged for every 15 min. The degradation efficiency of MB solution was analysed using UV-vis spectrometer (LAMBDA 25 UV/Vis Systems). Peaks were observed to be present between 600 to 700 nm. The conversion of MB solution can be calculated using the following equation:

$$R = \frac{(C_0 - C_t)}{C_0} \times 100\% \tag{1}$$

where C_0 represents the initial concentration of MB solution and C_t signifies concentration of MB solution during irradiation.

3 Results and discussion

3.1 XRD analysis

Fig. 1 illustrates the powder X-ray diffraction (XRD) pattern of synthesised TiO_2 NPs under different conditions. The sharp peaks obtained at 2θ values 25.3, 37.9, 48.4, 53.9, 55.3, 62.7, 70.1, 74.0 and 82.4 (PDF 98-005-9309) were equivalent to the planes (101), (004), (200), (105), (211), (204), (116), (215) and (303), indicated tetragonal structure of anatase TiO_2 nanoparticles. However, for TiO_2 NPs synthesised under acidic condition (pH 5), a weak diffraction peak at $2\theta = 31°$ (PDF 98-010-5395) due to (121) face of brookite phase with orthorhombic crystalline structure was observed. Besides, for uncalcined TiO_2 powder, a very broad peak around 25.5° was attributed to the characteristic diffraction peak of the amorphous state of TiO_2. Once the as-prepared TiO_2 powder was calcined, the intensity of
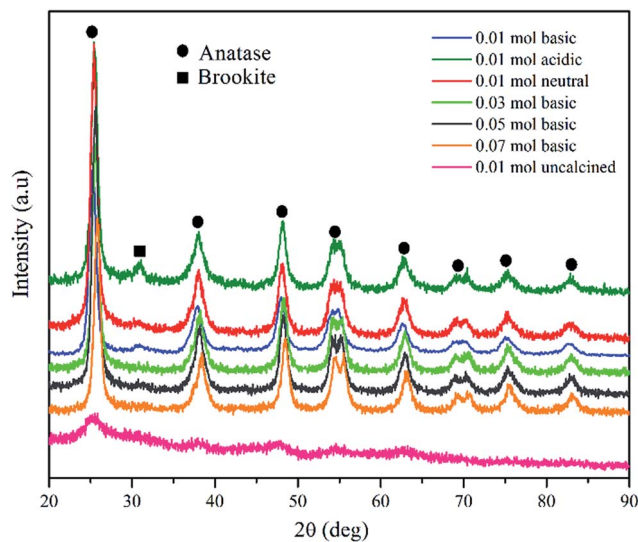
Fig. 1 X-ray patterns of TiO$_2$ NPs synthesised under different initial pH and concentration of TTIP.

XRD peaks became visible confirming that the TiO$_2$ powder underwent a calcination process. This confirms the occurrence of a transition from amorphous to crystalline anatase phase.

The average crystallite size, *d*-spacing, full-width at half maximum (FWHM) were determined using Rietveld refinement (Highscore Expert software). The influence of the concentration of TTIP and pH of initial solution on the crystallite sizes of the TiO$_2$ samples were listed in Table 1. The results show that with increasing TTIP concentration and reduction in the initial solution pH, the FWHM of the diffraction peak decreases and become narrower suggesting that the average crystallite size has become bigger correspondingly. This indicates that the enhancement of the crystallinity, stems from the increment of the crystalline volume ratio due to the size enlargement of the nuclei.[17]

3.2 N$_2$ adsorption and desorption analysis

The N$_2$ adsorption–desorption isotherms of the as-obtained TiO$_2$ NPs synthesised using different concentration of TTIP and initial solution pH are displayed in Fig. 2(a). Except for purchased pure anatase powder, all the curves exhibited the Type IV isotherm with H3 hysteresis loop of steep condensation

Table 1 Crystallographic parameters calculated by Rietveld refinement for TiO$_2$ NPs synthesised under various conditions. GOF: Goodness of Fit

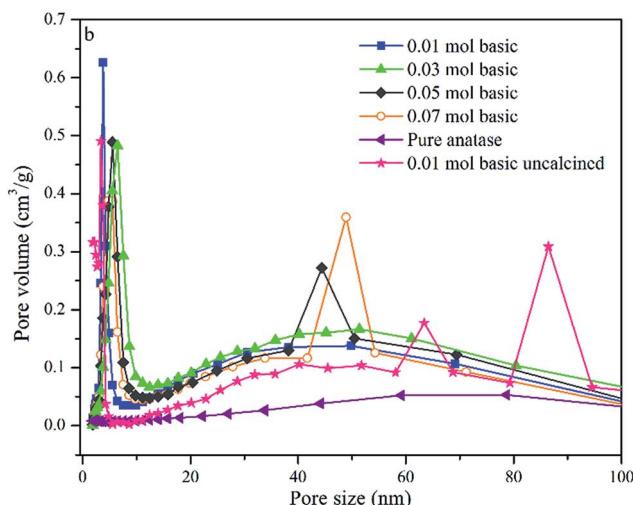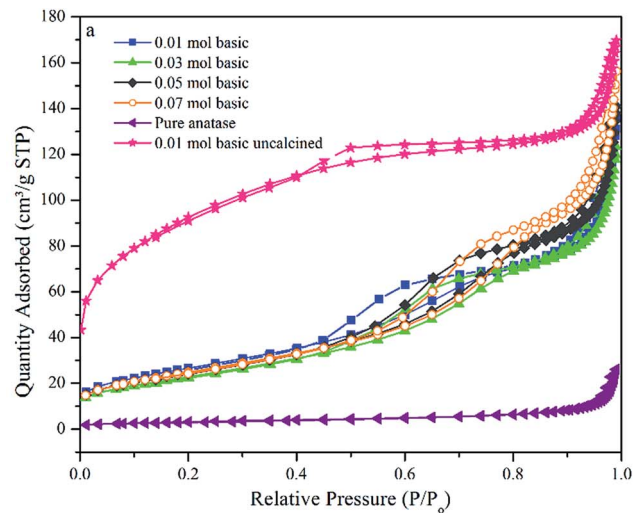| Samples	2θ (degree)	*d*-spacing	FWHM	Crystallite size (nm)	GOF
0.01 mol basic	25.4	3.49	0.980	8.9	1.90
0.01 mol neutral	25.3	3.52	0.969	11.6	1.89
0.01 mol acidic	25.5	3.49	0.831	12.2	1.26
0.03 mol basic	25.6	3.47	0.907	14.2	1.89
0.05 mol basic	25.7	3.48	0.839	14.3	1.46
0.07 mol basic	25.9	3.44	0.824	15.1	1.99

Fig. 2 (a) N$_2$ adsorption/desorption isotherm and (b) BJH pore size distribution TiO$_2$ NPs synthesised under different initial pH and concentration of TTIP.

at $P/P_0 = 0.4$–0.6, indicating existence of small mesopores. Isotherms with type H3 hysteresis loop suggest the presence of irregular long, slit-like narrow pores according to IUPAC classification. However, the condensation steep shifted to high relative pressure $P/P_0 = 0.9 - 1.0$, suggesting the occurrence of macropores.[16] The Barrett–Joyner–Halenda (BJH) pore size distribution for all synthesised samples as shown in Fig. 2(b), displayed the bimodal pore size distribution. As-prepared TiO$_2$ NPs (0.01 mol TTIP, pH 9) without calcination has the lowest average pore diameter of 3.4 nm with narrow distribution. This narrow pore size distribution remained with a slight increase in pore size (3.7 nm) after underwent calcination process. When the concentration of TTIP increased to 0.03 mol, 0.05 mol and 0.07 mol, the mean pore size increased to 4.8 nm, 5.5 nm and 6.5 nm, respectively with a broadened pore size distribution.

It is also interesting to note that Brunauer–Emmett–Teller (BET) specific surface area also changed with the amount of precursor used as shown in Table 2. It was observed that,

Table 2 Textural parameters and Langmuir–Hinselwood first-order constants for the degradation of MB by mesoporous TiO₂ NPs samples prepared with different concentration of TTIP and pH of initial solution

Concentration of precursor TTIP (mol)	Initial solution pH	BET ($m^2 g^{-1}$)	Crystallite size (nm)	k (min^{-1})	R^2
Pure anatase powder	—	10.4	—	0.079	0.997
0.01	9.0	87.2	8.9	0.169	0.996
0.01	7.0	81.6	11.6	0.048	0.976
0.01	5.0	72.9	12.2	0.036	0.979
0.03	9.0	80.8	14.2	0.028	0.984
0.05	9.0	80.1	14.3	0.016	0.980
0.07	9.0	78.5	15.1	0.015	0.977

surface area changed from 87.2 to 78.5 $m^2 g^{-1}$, which indicates that the increase in concentration of precursor decreases the surface area and subsequently resulting in an increase of the particle size of the samples. Moreover, the surface area of uncalcined TiO₂ was decreased from 309.7 to 87.2 $m^2 g^{-1}$ when the sample was introduced with high heating treatment. This is an indication of removal of organic template (starch) resulting in enlargement of pore size, which led to the decrease in surface area.[18,19] Also, it was verified that all the synthesised samples revealed higher BET surface area as compared to pure anatase nanopowder (10.4 $m^2 g^{-1}$).

3.3 UV-visible diffuse reflectance spectroscopy

The absorption spectra of all TiO₂ NPs synthesised samples using various concentrations of TTIP and different initial solution pH are shown in Fig. 3(a). A significant red shift in the band gap of TiO₂ NPs synthesised using 0.01 mol TTIP under basic condition were observed from the variation of $(\alpha h\nu)^2$ with photon energy ($h\nu$) compared to other samples. The extrapolated line drawn (Fig. 3(b)) for pure anatase and synthesised TiO₂ NPs corresponds to the bandgap of 3.20 and 3.00 eV, respectively. This suggests that the optical bandgap of the TiO₂ NPs has been reduced substantially compared to purchased pure anatase. In addition, e⁻ and h⁺ pairs can be generated, even though the particle is irradiated with longer wavelength-visible light.

Also, as shown in Fig. 3(a), the bandgaps of pure anatase, 0.01 mol (basic), 0.01 mol (neutral), 0.01 mol (acidic), 0.03 mol, 0.05 mol, 0.07 mol were determined to be 3.20, 3.00, 3.03, 3.07, 3.05, 3.07, and 3.07 eV, respectively. Therefore, by increasing the initial pH solution to basic the bandgaps of the products decreases accordingly. The decrease of bandgap could be due to the localized gap states induced by Ti³⁺ self-doping. This result also indicates that the concentration of Ti³⁺ in the TiO₂ products increased with increasing pH of initial solution (basic).[37] The existence of defects in the self – doped TiO₂ samples can further be confirmed by XPS analysis later.

3.4 Structures and morphologies

Fig. 4 displays the FESEM images of synthesised TiO₂ NPs under different concentration of TTIP and initial solution pH. FESEM image of Fig. 4(a) belongs to uncalcined TiO₂ sample where the particles are large and agglomerated. All samples exhibited

irregular spherical structures with rougher surfaces after the calcination process because calcination would enhance porous morphology for the as-synthesised TiO₂ NPs. From Fig. 4(b)–(d), it was observed that the particle size decreased as the pH of
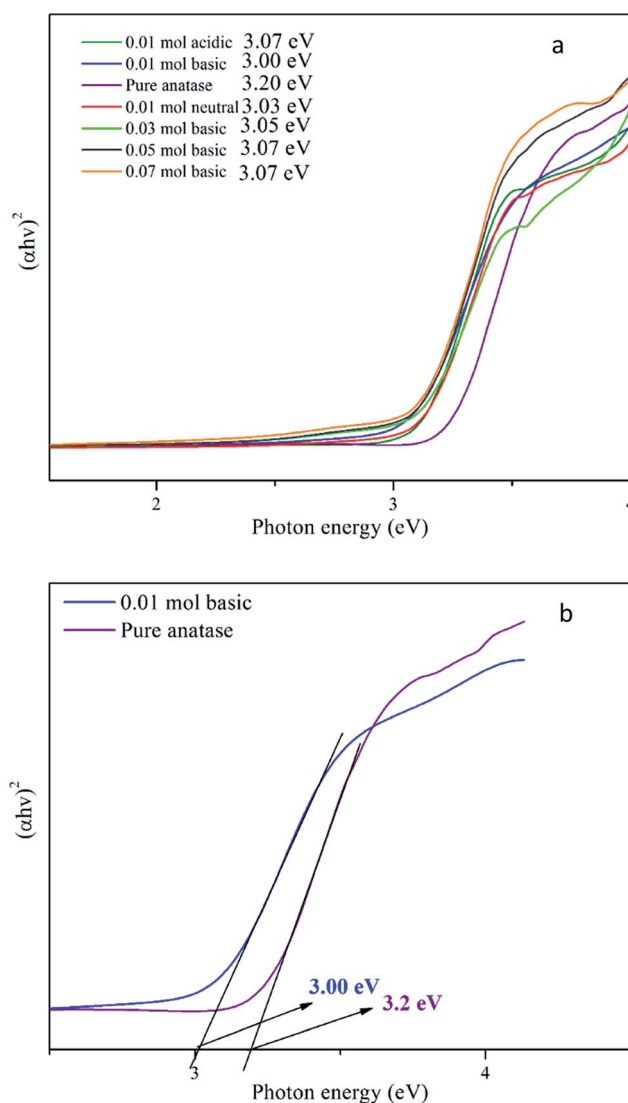

Fig. 3 (a) Bandgap of TiO₂ NPs synthesised using various concentration of TTIP and initial pH solution (b) compared bandgap spectra of synthesised sample and pure anatase.
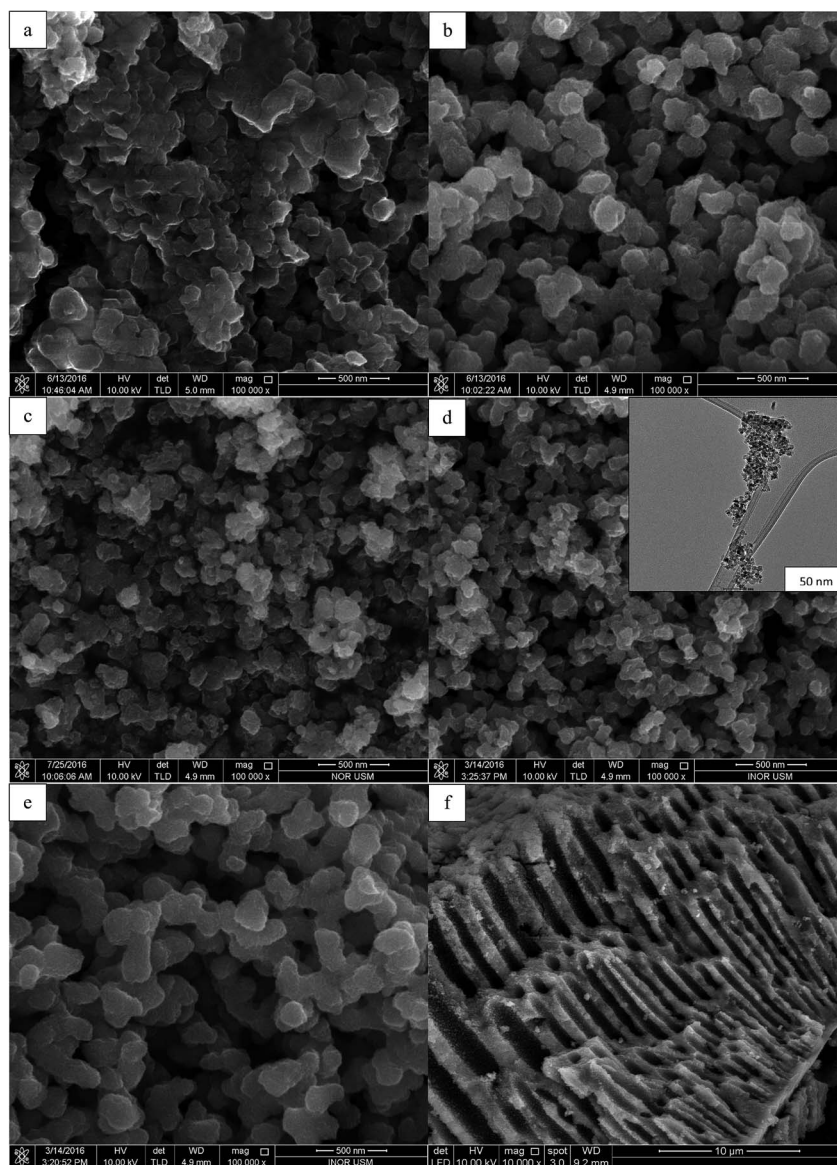
Fig. 4 FESEM micrographs (100 000×) of the TiO$_2$ NPs synthesised using (a) uncalcined TiO$_2$, (b) 0.01 mol TTIP, pH 5, (c) 0.01 mol TTIP, pH 7, (d) 0.01 mol TTIP, pH 9, insert: HRTEM image, (e) 0.07 mol TTIP pH 9, (f) pore channels of TiO$_2$ NPs (10 000×).

initial solution increased. Fig. 4(b) shows the morphology of sample synthesised using 0.01 mol TTIP under acidic condition (pH 5) has particle size of 99.2 ± 6.7 nm. When the pH of initial solution further increased to basic (pH 9), the particle size reduced drastically to 64.19 ± 2.6 nm. This is further confirmed with the HRTEM image (insert of Fig. 4(d)) which indicated that the size of synthesised TiO$_2$ NPs is in the nano range (20–70 nm). On the other hand, enlargement of particle size can be observed in Fig. 4(e) as the concentration of precursor was increased to 0.07 mol with diameter 80.20 ± 3.3 nm. This is due to enhanced coagulation and sintering resulting from the large concentration of TiO$_2$ nuclei generated at high TTIP precursor concentrations.[20,21]

Besides, the high-resolution SEM images could also give information on the meso or macroscopic properties. Fig. 4(f) demonstrates the extension of the irregular parallel-arrayed

long macro and mesoscopic channels through the material from the side view of the sample. Such open ended tube like channels could serve as ideal transport routes for introducing liquid phase into the interior of the framework of TiO$_2$.[18–21]

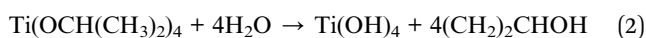### 3.5 Possible formation mechanism of mesoporous TiO$_2$

Although the exact formation mechanism of the mesoporous TiO$_2$ particles is not very clear, it is postulated that the soluble starch plays a key role in the formation of the mesoporous structures. Since starch is a polysaccharide carbohydrate, it can solubilise well in the boiling water. A dense formed when the starch granules swelled and burst, and the smaller amylose molecules started leaching out of the granules. Nucleation and initial crystal growth starts to take place when the precursor (Ti^{4+}) diffuse and form complexes with amylose molecules near
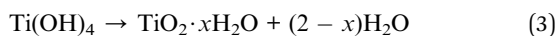
the interspaces between swollen starch microspheres. In most cases, the van der Waals interactions between the surface molecules of the nanocrystallites represent the driving force for self-assembly, and then TiO_2 can be assembled to form compact uniform nanoparticles around the inflated starch granules. After calcination at 500 °C for two hours, the swollen starch gel granule template was removed leaving mesoporous structures around the TiO_2 particles as illustrated in Scheme 1.[16,22]

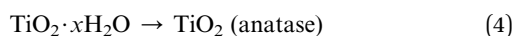Meanwhile, the reactions for the formation of anatase TiO_2 NPs are predicted as below:[23]

Hydrolysis:

$$Ti(OCH(CH_3)_2)_4 + 4H_2O \rightarrow Ti(OH)_4 + 4(CH_2)_2CHOH \quad (2)$$

Condensation:

$$Ti(OH)_4 \rightarrow TiO_2 \cdot xH_2O + (2 - x)H_2O \quad (3)$$

Crystallisation *via* calcination:

$$TiO_2 \cdot xH_2O \rightarrow TiO_2 \text{ (anatase)} \quad (4)$$

where x = number of water molecules.

TiO_2 nanoparticles were formed when titanium isopropoxides underwent hydrolysis and condensation. Initially, the hydrolysis process of titanium isopropoxides in an aqueous media occurred and titanium hydroxides ($Ti(OH)_4$) was formed as an intermediate as shown in eqn (2). $Ti(OH)_4$ is usually not stable and hence, it would go through the condensation process to produce amorphous hydrous oxide precipitates ($TiO_2 \cdot xH_2O$) as stated in eqn (3). The formed $TiO_2 \cdot xH_2O$ precipitates were then subjected to the calcination process at 500 °C to remove the water molecules to form the anatase crystalline TiO_2 NPs (eqn (4)) which were confirmed in the XRD pattern earlier.

3.6 XPS analysis

XPS analysis was further performed to investigate the chemical states of Ti and O in the synthesised TiO_2 NPs. The XPS spectrum Ti, O and C element without any impurities for TiO_2 NPs is shown in Fig. 4. The XPS spectra of Ti 2p and O 1s in Fig. 5(a) and (b) confirmed the chemical compositions of TiO_2. For the Ti 2p spectra, two primary peaks are attributed to the characteristic Ti $2p_{1/2}$ and Ti $2p_{3/2}$ peaks of Ti^{4+}. The symmetric curve

with a binding energy located at 458.7 and 464.3 eV is in agreement with that of Ti^{4+} $2p_{3/2}$ and Ti^{4+} $2p_{1/2}$ in TiO_2, respectively.[24]

Besides, the Ti 2p peaks were deconvoluted into another two peaks: Ti^{3+} $2p_{3/2}$ at 457.9 eV and Ti^{3+} $2p_{1/2}$ at 463.3 eV which can be claimed as self-doped TiO_2 with the presence of Ti^{3+}. Zhou *et al.*[25] and Mai W. *et al.*[26] reported that TiO_2 surface defects (Ti^{3+}) played a significant role as they are active sites for oxygen adsorption and for trapping the electron to prevent the recombination of electrons and holes. In addition, surface Ti^{3+} sites also reduced the bandgap of TiO_2 NPs and provided the unique activity and selectivity in the target reactions at relatively high wavelengths. Ti^{4+} reduction to Ti^{3+} is usually accompanied by vacuum annealing or thermal treatment (calcination). Self-doped TiO_2 can also be generated by the carbon formed from pyrolysis of titanyl organic compounds. In the calcination process, Ti^{4+} ions accept electrons from these reducing gases or lattice oxygens which are usually removed from stoichiometric TiO_2. At low temperature (300 °C), hydrogen interacted physically with adsorbed oxygen on the surface of TiO_2. When the thermal temperature was raised higher than 300 °C, electrons were transferred from the H atoms to the O atoms in the lattice of TiO_2. Then, the oxygen vacancies were formed when the O atom left with the H atom in the form of H_2O. The interface between H_2 and TiO_2 progressed more significantly as the calcination temperature increased up to 450 °C, in which the electrons transferred from oxygen vacancies to Ti^{4+} ions, and then Ti^{3+} ions were formed. In this study, the synthesised TiO_2 NPs was calcined at 500 °C, hence, more Ti^{3+} ions were produced rather than formation of oxygen vacancies (where the oxygen vacancy XPS peaks invisible in the result obtained). Meanwhile, the possible mechanism for the reduction reaction caused by the pyrolysis of titanyl organic compounds is that the carbon from organic component carbonizing could reduce Ti^{4+} to Ti^{3+} at high temperature. Basically, the reduction process of Ti^{4+} to Ti^{3+} takes place due to the reduction by electron donors such as H_2, C, or lattice oxygen in TiO_2.[25] In the O 1s spectrum, only two peaks at binding energies 529.3 eV, and 530.2 eV are observed which are attributed to lattice oxygen and surface adsorbed OH group.[27]

The C 1s spectrum (Fig. 5(c)) includes a strong peak at 284.6 eV and a shoulder at 288.0 eV. These features correspond to two forms of carbon species in the sample. The peak at
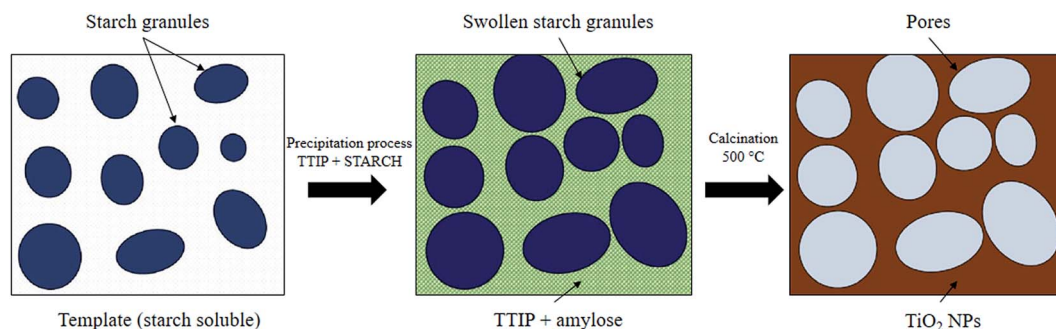
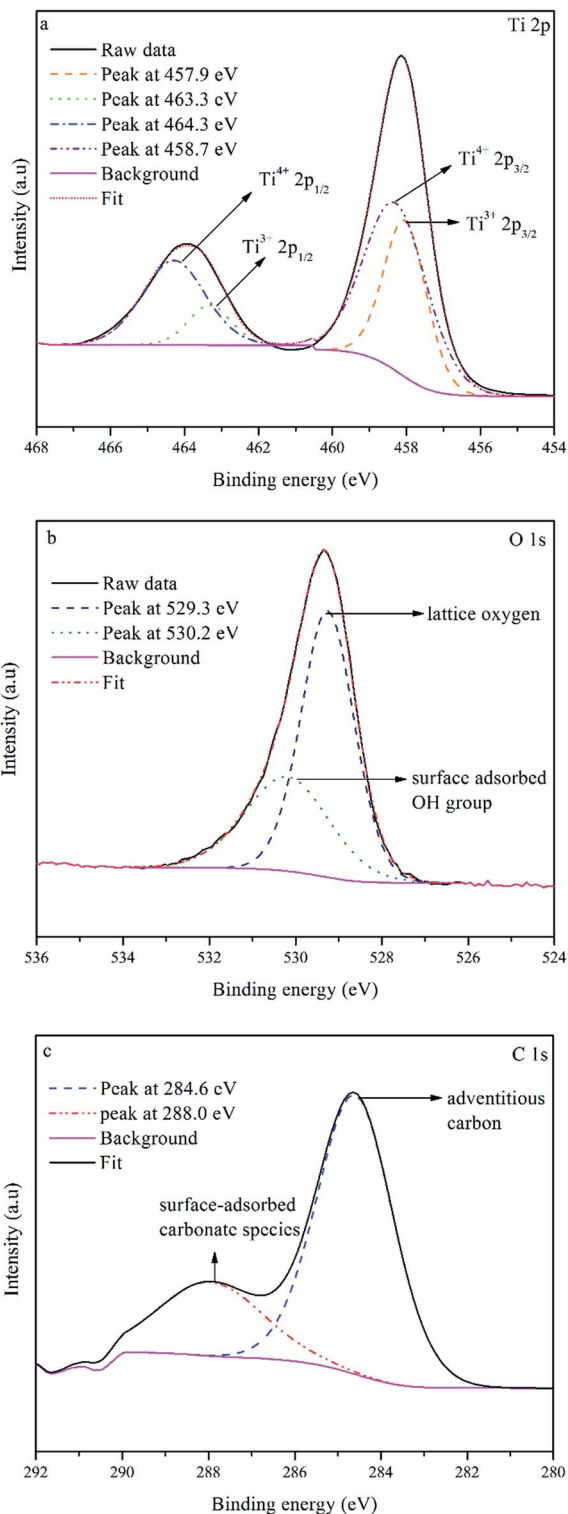**Scheme 1** Possible formation of pores in TiO_2 NPs.

Fig. 5 High-resolution XPS spectra of (a) Ti 2p, (b) O 1s and (c) C 1s of synthesised TiO$_2$ NPs using 0.01 mol TTIP under basic condition.

284.6 eV on the XPS spectra is associated with elemental carbon from organic impurities in the environment that were adsorbed onto the surface of TiO$_2$ and the peak at 288.0 eV is associated with surface-adsorbed carbonate species resulting from carbon residues on the surface of TiO$_2$.[28] Besides, it is also proven that

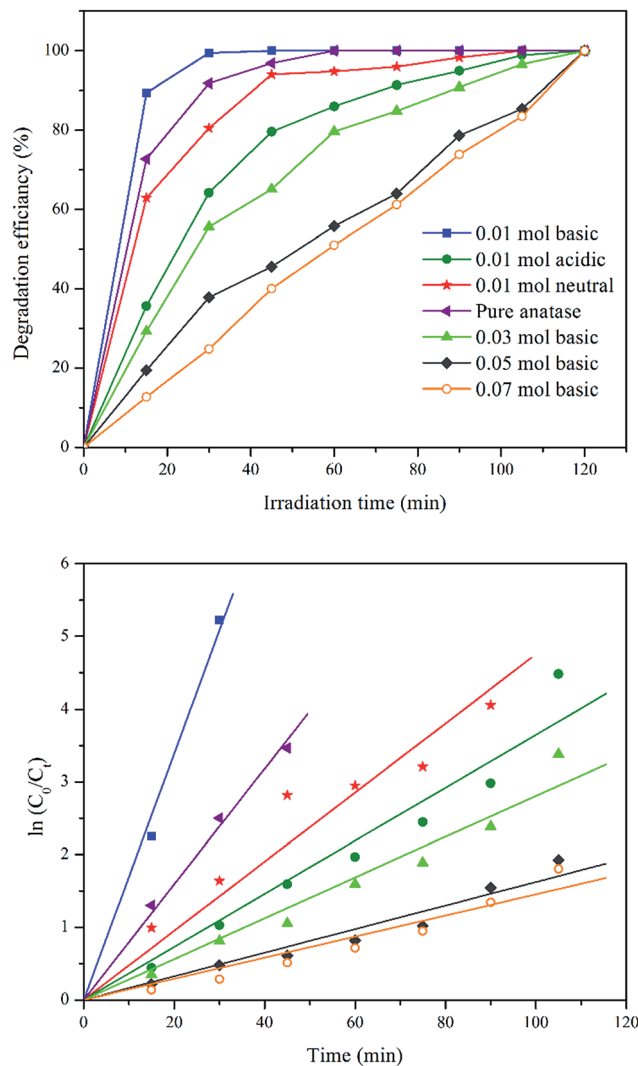
Fig. 6 Degradation efficiency and first-order kinetics for TiO$_2$ NPs synthesised using different TTIP concentration and initial solution pH.

TiO$_2$ NPs synthesised showed no carbon doped material originated from the starch, since peak 282.0 eV which assigned to Ti–C bond is absent in the obtained XPS spectrum. Thus, from the XPS result, self-doped TiO$_2$ NPs is the possible factor that the photocatalytic activity occurred near to visible range than at UV range.

3.7 Photocatalytic activity and kinetic studies of TiO$_2$ NPs

3.7.1 Effect of TTIP concentration and initial solution pH.

The photodegradation of methylene blue (MB) dye was used in order to demonstrate their potential environmental application. Fig. 6 shows the degradation rate and the pseudo-first order rate constants of the photocatalyst system were estimated from the slopes of linear plots $\ln(C_0/C_t)$ versus time. The reaction rate constants (k) were calculated according to the Langmuir–Hinshelwood first order rate model which is generally used for photocatalytic degradation process when the initial concentration of pollutant is low,

$$\ln\left(\frac{C_0}{C_t}\right) = kt \tag{5}$$

where C_0 and C_t are the concentrations of MB aqueous solution at irradiation times of 0 and t min, respectively.

According to Table 2, the activity of the synthesised TiO_2 photocatalyst decreased in order 0.01 mol basic > purchased pure anatase > 0.01 mol neutral > 0.01 mol acidic > 0.03 mol basic > 0.05 mol basic > 0.07 mol basic. The photoreactivity experiments have shown that MB photodegradation depends on the particle size of the TiO_2 powders. Since the concentration of TTIP increased from 0.01 mol to 0.07 mol and the initial solution pH reduced from 9.0 (basic) to 5.0 (acidic), the degradation rate reduced from 0.169 to 0.015 min^{-1} and from 0.169 to 0.036 min^{-1}, respectively. These results suggest that as we increased the concentration of TTIP and reduced the initial solution pH, incomplete nucleation occurred due to supersaturation of solution which led to the increase in particle size and hence, decrease in the specific surface area of as-synthesised powder, indirectly reducing the photocatalytic degradation efficiency of MB solution. Besides, an increase in crystallite size of synthesised TiO_2 NPs under various concentrations of TTIP and initial solution pH (obtained from XRD data), reduces the photocatalytic activity.[18,29]

3.7.2 Effect of catalyst dosage. In order to study the effect of catalyst dosage on degradation kinetics of MB solution, different amounts of TiO_2 NPs (0.05, 0.10, 0.20 or 0.40 g) synthesised using 0.01 mol TTIP under basic condition were employed (shown in Fig. 7). The regression correlation coefficients (Langmuir–Hinselwood constant; R^2), together with the calculated kinetics data of the photodegradation of MB, are given in Table 3. The result demonstrated that degradation rate decreased from 0.169 to 0.069 min^{-1} as the catalyst loading into MB solution increased from 0.1 to 0.4 g. This means that the relative efficiency of the catalyst is lowered and a limiting rate is achieved when high amounts of TiO_2 NPs are used. One possible explanation for such behaviour is that when the photocatalyst amount surpassed 0.1 g, part of the catalyst surface probably became unavailable for photon absorption and dye adsorption under such conditions or deactivation of activated molecules by collision with ground state molecules may occur at higher catalyst loading and thus, bringing little stimulation to catalytic reaction.[30,31] However, the catalyst dosage was further decreased to 0.05 g to determine its degradation efficiency. It is clear that the rate of degradation decrease proportionally with the decrease in the amount of the catalyst. This due to the available number of photocatalyst active sites can be insufficient for adsorption to a greater number of dyes.

3.7.3 Effect of initial dye concentration. Fig. 8 shows the degradation rate of dye measured under different concentrations of dye MB solution (6, 10, 20 and 40 ppm) with optimum catalyst loading (0.1 g TiO_2 NPs). The regression correlation coefficients (R^2) were obtained and the kinetics data of the photodegradation of MB were calculated and given in Table 4. The possible explanation for this behaviour is that as the initial concentration of the dye increases, the formation of intermediates increased during the course of reaction. Hence,
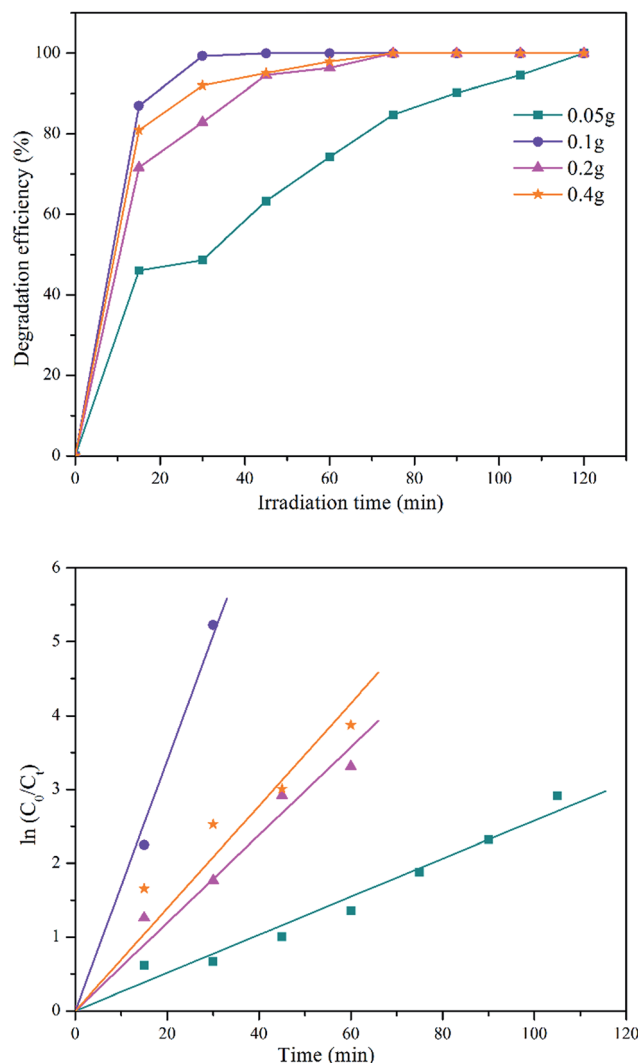

Fig. 7 Effect of catalyst dosage plot of MB removal percentage against irradiation time using different catalyst dosage and its first-order kinetic plots.

competition starts between the intermediates and the dye molecules for surface active sites of TiO_2 NPs leading to restriction of light penetration to the surface of the catalyst. This phenomenon indirectly reduces the degradation rate of MB solution at high concentration. Besides, the active sites of photocatalyst will be completely occupied by the dye molecules leading to the decrease in the generation of OH radicals and thus, inhibit the degradation process from occurring between

Table 3 First-order constants for the photodegradation of MB solution at different catalyst dosage

Catalyst dosage (g)	k (min^{-1})	R^2
0.05	0.026	0.9870
0.1	0.169	0.9967
0.2	0.059	0.9860
0.4	0.069	0.9757

dye molecules and TiO$_2$ NPs.[28,32,33] TiO$_2$ NP synthesised in present work has two folds better photocatalytic activity compared to the ZnO synthesised by Zhang and his co-workers.[16] ZnO acquired 240 min to degrade 5 mg L^{-1} of rhodamine B (RhB). Meanwhile, TiO$_2$ NPs synthesised using similar method as ZnO could degrade 6 mg L^{-1} of MB solution in 45 minutes. Besides, several studies showed that the rate of degradation of methylene blue (low concentration: <10 ppm) is very low compared to photocatalytic activity of TiO$_2$ NPs in this study.[18–20,28,30,34]

3.7.4 Regeneration and reusability of TiO$_2$ NPs. Ten cycles of photocatalytic activities were carried out to evaluate the stability of TiO$_2$ NPs (Fig. 9) after regeneration process. For each new cycle, the synthesised photocatalyst was washed in boiling distilled water for 15 min and oven dried overnight at 100 °C. After 10 cycles, the degradation efficiency of MB reduced only about 13.3% from 100% to 86.7%. The results revealed that the photocatalytic activity of TiO$_2$ NPs photocatalyst has a good

Table 4 Kinetic constants for the photodegradation of MB solution at different initial dye concentration

Initial dye concentration (ppm)	k (min^{-1})	R^2
6	0.169	0.9967
10	0.046	0.9934
20	0.028	0.9757
40	0.009	0.9765

repeatability. The high stability of TiO$_2$ NPs in powder form generates a high photocatalytic activity, makes its separation from reaction solution quite difficult. The reduction in the degradation efficiency after 10 catalytic cycles, can be explained by the material loss during the recovering procedure because of the difficulty to avoid any loss of catalyst materials during the washing and filtration process.[32–35]

After ten cycles of reusability test, TiO$_2$ NPs were analysed using XRD and FESEM to determine its phase, porosity and morphology stability. Fig. 10 showed XRD spectra of recycled TiO$_2$ NPs for ten times and freshly synthesised TiO$_2$ NPs. Based on the Fig. 10, synthesised TiO$_2$ NPs remained same as in anatase phase after ten washings. As it can be seen, the intensity of the peak belongs to anatase phase $2\theta = 25.6°$ increased due to the heat treatment introduced after washing process for every cycle for overnight. Generally, heat treatment at high temperature could induce the crystallinity and phase transition of metal oxides.[36,37] In this case, only increase in crystallinity was observed as the temperature used for each cycle was 100 °C. FESEM was used to analyse the surface morphology and porosity of TiO$_2$ NPs after ten recycles. Fig. 11(a–c) showed the ordered TiO$_2$ porous structures at different magnifications after 10 cycles of photocatalytic activities. The reused TiO$_2$ NPs still exhibited irregular parallel-arrayed long macro and mesoscopic channels through the material from the side view of the sample. No changes were observed on the walls of the TiO$_2$ NPs since
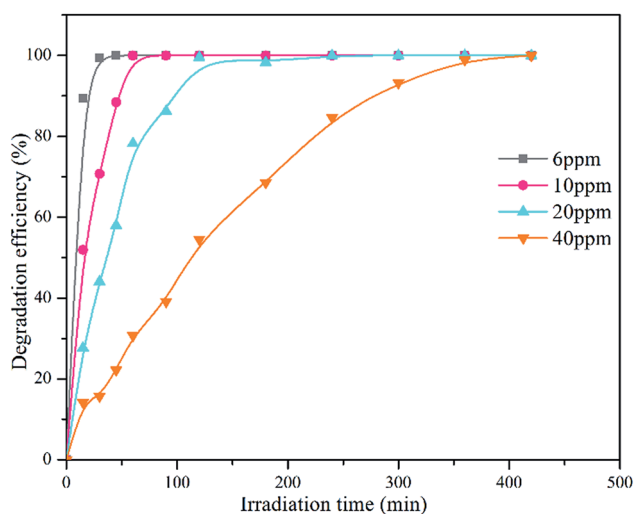

Fig. 8 Degradation efficiency of different initial concentration of MB solution and its first-order kinetic model plot.
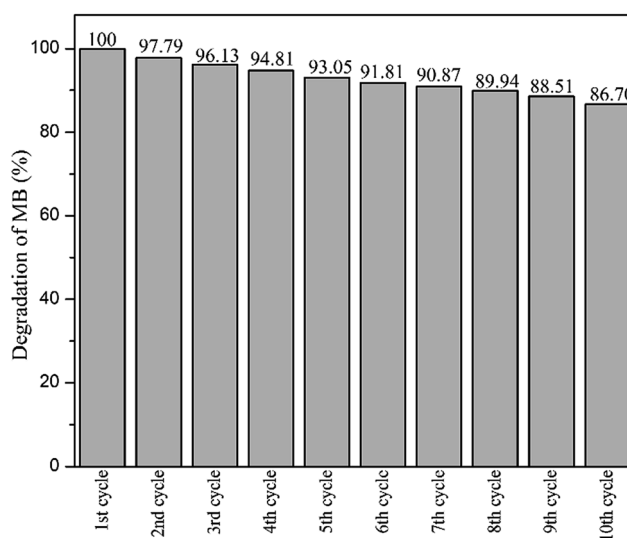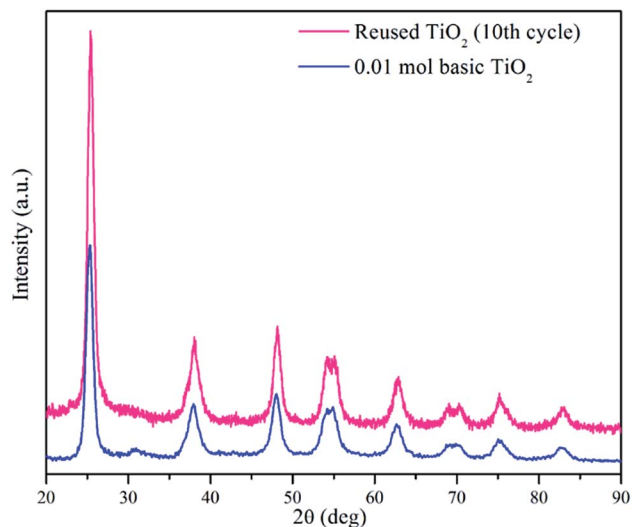

Fig. 9 Reusability test of synthesised TiO$_2$ NPs.

Fig. 10 XRD spectra of TiO_2 NPs after ten recycles.

TiO_2 surface was composed of pores. Besides, the particle size of recycled of TiO_2 NPs increased slightly to 68.83 ± 4.4 nm compared to the freshly synthesised TiO_2 NPs (64.19 ± 2.6 nm). The slight increase in particle size might cause by the heating process in overnight during every cycle.[38] Hence, we can conclude that the reusability test using boiling water in the washing process does not affect the stability of the TiO_2

NPs in term of morphology, phase and porosity of the metal oxide.

3.8 Photocatalytic reaction mechanism of Ti^{3+} surface defects

TiO_2 with surface defects enhances the photocatalytic activity by introducing a local state at the bottom of the conduction band (CB) in the range of 0.75 eV–1.18 eV so that it extends the photoresponse of TiO_2 from UV to visible light region. As a kind of defect, Ti^{3+} acts as an electron trap and results in the reduction of an electron hole pair recombination rate, thereby the subsequent reactions caused by the electrons and holes were dramatically improved.[39] In this case, electrons donors reacted with holes. The electron can be trapped by Ti^{4+} to generate an isolated Ti^{3+} ion as shown in eqn (6). In the presence of O_2, the Ti^{3+} sites easily react with O_2, leading to the formation of radicals such as $^{\cdot}O_2^{-}$, $HO_2^{\cdot}$, and $^{\cdot}OH$ as shown in eqn (7) and (8). These $^{\cdot}OH$ and $O_2^{\cdot-}$ species are able to degrade the MB molecules in solution. These $^{\cdot}OH$ and $O_2^{\cdot-}$ species are able to assist in the degradation of the MB molecules in solution. $^{\cdot}OH$ species reacts with H^+ ion to produce hydrogen peroxide (H_2O_2) as stated in eqn (9). The H_2O_2 is then reacted with the electron (e_{cb}^{-}) from TiO_2 and subsequently increases the concentration of $^{\cdot}OH$ radical to enhance the degradation process as shown in eqn (10).

Meanwhile, the photogenerated holes due to transition of electron from valance band (VB) to the local state by Ti^{3+} have
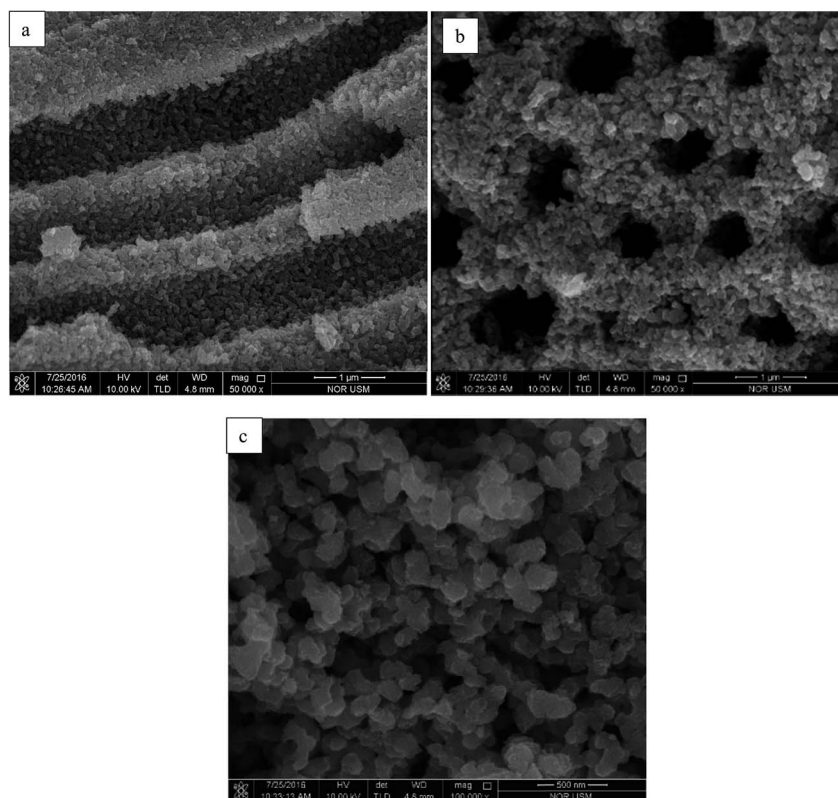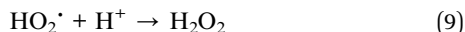

Fig. 11 FESEM micrographs of recycled TiO_2 NPs (a) pore channels of TiO_2 NPs, (b) pores on the surface of TiO_2 after 10 cycles and (c) magnified TiO_2 NPs.

strong oxidation ability and can directly degrade MB to produce less harmful products such as water and carbon dioxide.[40,41] The charge transfer processes occurred in TiO_2 with surface defect may be as follows:[38–41]

$$e_{cb}^- + Ti^{4+}OH \rightarrow Ti^{3+}OH \tag{6}$$

$$Ti^{3+}OH + O_2 \rightarrow Ti^{4+}OH + {}^{\cdot}O_2^- \tag{7}$$

$${}^{\cdot}O_2^- + H^+ \rightarrow HO_2{}^{\cdot} \tag{8}$$

$$HO_2{}^{\cdot} + H^+ \rightarrow H_2O_2 \tag{9}$$

$$H_2O_2 + e_{cb}^- \rightarrow {}^{\cdot}OH + OH^- \tag{10}$$

4 Conclusions

This study outlined the development of TiO_2 nanoparticles *via* green technique. Active mesoporous anatase TiO_2 NPs with small crystallite size (9 nm) was successfully synthesised using titanium tetraisopropoxide (TTIP) as the precursor, water as the solvent, and starch as the template using a low temperature precipitation method. The photocatalytic activities of prepared TiO_2 photocatalyst were evaluated using methylene blue (MB) aqueous solution at 6 ppm. The results clearly indicated that the sample synthesised using 0.01 mol TTIP under basic condition has smaller particle sizes (64.19 ± 2.6 nm) and higher specific area (87.2 m^2 g^{-1}) which contributed to better photocatalytic performance. XPS analysis indicates that TiO_2 NPs is active at near to visible range than the UV range is highly attributed to self-doped (Ti^{3+}) of TiO_2 than the carbon-doped from starch employed in this green method. It was found that degradation kinetics of MB fitted the Langmuir–Hinselwood first order kinetics. The rate of photodegradation of MB solution decreased when the concentration of precursor increased and the initial pH of solution decreased. The optimum condition for photodegradation of MB solution at 6 or 10 ppm MB solution is by using 0.1 g TiO_2 NPs synthesised using 0.01 mol TTIP under basic condition. Besides, synthesised TiO_2 NPs revealed high stability against photodegradation process as it can be recycled up to 10 cycles. The method developed in this work is fast and environmentally friendly for the preparation of mesoporous TiO_2 NPs powders with good photocatalytic activities.

Conflicts of interest

There are no conflicts to declare.

Acknowledgements

Notes and references

1 Y. Ju, M. Wang, Y. Wang, S. Wang and C. Fu, Electrical properties of amorphous titanium oxide thin films for bolometric Application, *Adv. Condens. Matter Phys.*, 2013, 100.

2 S. Qiu and S. J. Kalita, Synthesis, processing and characterization of nanocrystalline titanium dioxide, *Mater. Sci. Eng., A*, 2006, **327**, 435–436.

3 W. A. Daoud and W. S. Tung, Self-cleaning fibers *via* nanotechnology – a virtual reality, *J. Mater. Chem.*, 2011, **21**, 7858–7869.

4 D. Tang and G. Zhang, Ultrasonic-assistant fabrication of cocoon-like Ag/AgFeO$_2$ nanocatalyst with excellent plasmon enhanced visible-light photocatalytic activity, *Ultrason. Sonochem.*, 2017, **37**, 208–215.

5 Z. Wan, G. Zhang, X. Wu and S. Yin, Novel visible-light-driven Z-scheme Bi$_{12}$GeO$_{20}$/g-C$_3$N$_4$ photocatalyst: oxygen-induced pathway of organic pollutants degradation and proton assisted electron transfer mechanism of Cr(VI) reduction, *Appl. Catal., B*, 2017, **207**, 17–26.

6 M. Pelaez, N. T. Nolan, S. C. Pillai, M. K. Seery, P. Falaras, A. G. Kontos, *et al.*, A review on the visible light active titanium dioxide photocatalysts for environmental applications, *Appl. Catal., B*, 2012, **125**, 3331–3349.

7 D. Wu, M. Long, J. Zhou, W. Cai, X. Zhu, C. Chen, *et al.*, Synthesis and characterization of self-cleaning cotton fabrics modified by TiO$_2$ through a facile approach, *Surf. Coat. Technol.*, 2009, **203**, 3728–3733.

8 M. Montazer and E. Pakdel, Functionality of nano titanium dioxide on textiles with future aspects: focus on wool, *J. Photochem. Photobiol., C*, 2011, **12**, 293–303.

9 C. Colleoni, M. R. Massafra and G. Rosace, Photocatalytic properties and optical characterization of cotton fabric coated *via* sol–gel with non-crystalline TiO$_2$ modified with poly(ethylene glycol), *Surf. Coat. Technol.*, 2012, **207**, 79–88.

10 K. Kądzioła, I. Piwoński, A. Kisielewska, D. Szczukocki, B. Krawczyk and J. Sielski, The photoactivity of titanium dioxide coatings with silver nanoparticles prepared by sol–gel and reactive magnetron sputtering methods – comparative studies, *Appl. Surf. Sci.*, 2014, **288**, 503–512.

11 Z. Tan, K. Sato and S. Ohara, Synthesis of layered nanostructured TiO$_2$ by hydrothermal method, *Adv. Powder Technol.*, 2014, **26**, 296–302.

12 S. K. Tripathy, T. Sahoo, M. Mohapatra, S. Anand and Y. T. Yu, Polyol-assisted synthesis of TiO$_2$ nanoparticles in a semi-aqueous solvent, *J. Phys. Chem. Solids*, 2009, **70**, 147–152.

13 J. Morales, A. Maldonado and M. D. L. Olvera, Synthesis and characterization of nanostructured TiO$_2$ anatase-phase powders obtained by the homogeneous precipitation method, *10th International Conference on Electrical Engineering*, Computing Science and Automatic Control (CCE), Mexico City, 30 September–4 October 2013, pp. 391–394.

14 M. N. Nadagouda, Green synthesis of nanocrystals and nanocomposites, *Mod. Aspects Bulk Cryst. Thin Film Prep.*, 2012, 395–412.

15 A. K. Maratha, Green technique-solvent free synthesis and its advantages, *Int. J. Res. Ayurveda Pharm.*, 2011, **2**, 1079–1086.

16 G. Zhang, X. Shen and Y. Yang, Facile synthesis of monodisperse porous ZnO spheres by a soluble starch-assisted method and their photocatalytic activity, *J. Phys. Chem. C*, 2011, **115**, 7145–7152.

17 M. Gharagozlou, Influence of calcination temperature on structural and magnetic properties of nanocomposites formed by Co-ferrite dispersed in sol–gel silica matrix using tetrakis (2-hydroxyethyl) orthosilicate as precursor, *Chem. Cent. J.*, 2011, **5**, 19.

18 D. Zhang and G. Li, Al_2O_3-enhanced Macro/Mesoporous Fe/TiO_2 for Breaking Down Nitric Oxide, *Chem., Emiss. Control, Radioact. Pollut. Indoor Air Qual.*, 2014, **2011**, 2–14.

19 E. Y. Kim, D. S. Kim and B. T. Ahn, Synthesis of mesoporous TiO_2 and Its application to photocatalytic activation of Methylene Blue and *E. coli*, *Bull. Korean Chem. Soc.*, 2009, **30**, 193–196.

20 X. Wang, J. C. Yu, C. Ho, Y. Hou and X. Fu, Photocatalytic activity of a hierarchically macro/mesoporous titania, *Langmuir*, 2005, **21**, 2552–2559.

21 C. S. Kim, K. Nakaso, B. Xia, K. Okuyama and M. Shimada, A new observation on the phase transformation of TiO_2 nanoparticles produced by a CVD method, *Aerosol Sci. Technol.*, 2005, **39**, 104–112.

22 L. Q. Tang, W. Ni, H. Y. Zhao, Q. Xu and J. X. Jiao, Preparation of macroporous TiO_2 by starch microspheres template with assistance of supercritical CO_2, *BioResources*, 2009, **4**, 38–48.

23 S. Mahshid, Synthesis of TiO_2 nanoparticles by hydrolysis and peptization of titanium isopropoxide solution, *J. Mater. Process. Technol.*, 2007, **189**, 296–300.

24 B. Bharti, S. Kumar, H.-N. Lee and R. Kumar, Formation of oxygen vacancies and Ti^{3+} state in TiO^2 thin film and enhanced optical properties by air plasma treatment, *Sci. Rep.*, 2016, **6**, 1–12.

25 Y. Zhou, C. Chen, N. Wang, Y. Li and H. Ding, Stable Ti^{3+} self-doped Anatase-Rutile mixed TiO_2 with enhanced visible light utilization and durability, *J. Phys. Chem. C*, 2016, **11**, 6116–6124.

26 W. Mai, F. Wen, D. Xie, Y. Leng and Z. Mu, Structure and composition study of carbon-doped titanium oxide film combined with first principles, *J. Adv. Ceram.*, 2014, **1**, 49–55.

27 L. XiongBin, J. L. Li, B. Yang and Y. Yu, Ti^{3+} in the surface of titanium dioxide: Generation, properties and photocatalytic application, *J. Nanomater.*, 2012, 1–12.

28 K. Li, Z. Huang, X. Zeng, B. Huang, S. Gao and J. Lu, Synergetic Effect of Ti^{3+} and Oxygen Doping on Enhancing Photoelectrochemical and Photocatalytic Properties of TiO_2/g-C_3N_4 Heterojunctions, *ACS Appl. Mater. Interfaces*, 2017, **9**(13), 11577–11586.

29 M. D. G. de Luna, J. C. Lin Te, M. J. N. Gotostos and M. C. Lu, Photocatalytic oxidation of acetaminophen using carbon self-doped titanium dioxide, *Sustainable Environ. Res.*, 2016, **4**, 161–167.

30 A. Zyoud, A. Zu'bi, M. H. S. Helal, D. Park, G. Campet and H. S. Hilal, Optimizing photo-mineralization of aqueous methyl orange by nano-ZnO catalyst under simulated natural conditions, *J. Environ. Health Sci. Eng.*, 2015, **13**, 46.

31 S. K. Kavitha and P. N. Palanisamy, Photocatalytic and Sonophotocatalytic Degradation of Reactive Red 120 using Dye Sensitized TiO_2 under Visible Light, *J. Eng. Technol.*, 2011, 1–6.

32 R. J. Tayade, T. S. Natarajan and H. C. Bajaj, Photocatalytic degradation of Methylene Blue dye using ultraviolet light emitting diodes, *Ind. Eng. Chem. Res.*, 2009, **48**, 10262–10267.

33 U. G. Akpan and B. H. Hameed, Parameters affecting the photocatalytic degradation of dyes using TiO_2-based photocatalysts: A review, *J. Hazard. Mater.*, 2009, **170**, 520–529.

34 M. A. M. Salleh, D. K. Mahmoud, W. A. W. A. Karim and A. Idris, Cationic and anionic dye adsorption by agricultural solid wastes: A comprehensive review, *Desalination*, 2011, **280**, 1–13.

35 C. Randorn, J. T. S. Irvine and P. Robertson, Synthesis of visible-light-activated yellow amorphous TiO_2 photocatalyst, *Int. J. Photoenergy*, 2008, 1–6.

36 S. M. Lam, J. C. Sin and A. R. Mohamed, Parameter effect on photocatalytic degradation of phenol using TiO_2-P25/activated carbon (AC), *Korean J. Chem. Eng.*, 2010, **27**, 1109–1116.

37 Y. Chen and D. D. Dionysiou, Effect of calcination temperature on the photocatalytic activity and adhesion of TiO_2 films prepared by the P-25 powder-modified sol–gel method, *J. Mol. Catal. A: Chem.*, 2006, **244**, 73–82.

38 M. M. Khan, S. A. Ansari, D. Pradhan, M. O. Ansari, D. H. Han, J. Lee, *et al.*, Band gap engineered TiO_2 nanoparticles for visible light induced photoelectrochemical and photocatalytic studies, *J. Mater. Chem. A*, 2014, **2**, 637–644.

39 H. Lin, C. P. Huang, W. Li, C. Ni, S. I. Shah and Y. H. Tseng, Size dependency of nanocrystalline TiO_2 on its optical property and photocatalytic reactivity exemplified by 2-chlorophenol, *Appl. Catal., B*, 2006, **68**, 1–11.

40 L. B. Xiong, J. L. Li, B. Yang and Y. Yu, Ti^{3+} in the surface of titanium dioxide: Generation, properties and photocatalytic application, *J. Nanomater.*, 2012, 1–13.

41 L. Ma, I. Jia, X. Guo and L. Xiang, Current status and perspective of rare earth catalytic materials and catalysis, *Chin. J. Catal.*, 2014, **35**, 108–119.